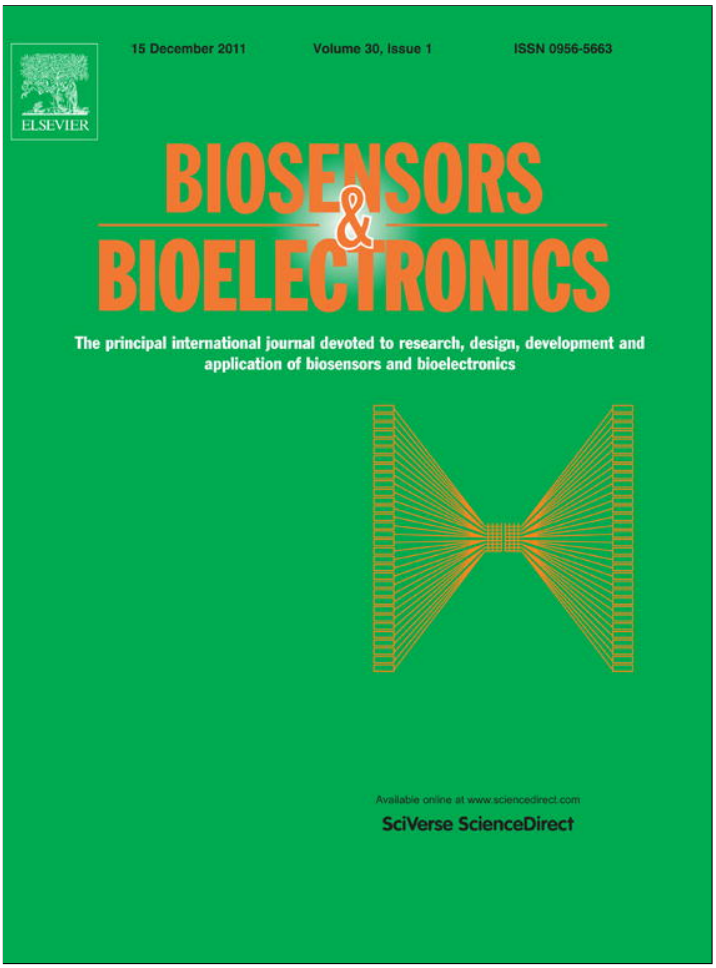

Biosensors and Bioelectronics 30 (2011) 13–20

Contents lists available at ScienceDirect

Biosensors and Bioelectronics

journal homepage: www.elsevier.com/locate/bios

Modeling and development of a low frequency contactless dielectrophoresis (cDEP) platform to sort cancer cells from dilute whole blood samples

Michael B. Sano[a,c], John L. Caldwell[b,c], Rafael V. Davalos[a,c,*]

[a] School of Biomedical Engineering and Sciences Virginia Tech–Wake Forest University, Blacksburg, VA 24061, United States
[b] Bradley Department of Electrical and Computer Engineering, Virginia Tech, Blacksburg VA 24061, United States
[c] Bio-Electro-Mechanical Systems Laboratory, Institute for Critical Technology and Applied Science (ICTAS), Virginia Tech, VA 24061, United States

ARTICLE INFO

Article history:
Received 8 June 2011
Received in revised form 18 July 2011
Accepted 20 July 2011
Available online 9 August 2011

Keywords:
Electrokinetics
Enrichment
Selective isolation
Cancer detection
Lab on a chip

ABSTRACT

Contactless dielectrophoresis (cDEP) devices are a new adaptation of dielectrophoresis in which fluid electrodes, isolated from the main microfluidic channel by a thin membrane, provide the electric field gradients necessary to manipulate cells. This work presents a continuous sorting device which is the first cDEP design capable of exploiting the Clausius-Mossotti factor at frequencies where it is both positive and negative for mammalian cells. Experimental devices are fabricated using a cost effective technique which can achieve 50 μm feature sizes and does not require the use of a cleanroom or specialized equipment. An analytical model is developed to evaluate cDEP devices as a network of parallel resistor-capacitor pairs. Two theoretical devices are presented and evaluated using finite element methods to demonstrate the effect of geometry on the development of electric field gradients across a wide frequency spectrum. Finally, we present an experimental device capable of continuously sorting human leukemia cells from dilute blood samples. This is the first cDEP device designed to operate below 100 kHz resulting in successful manipulation of human leukemia cells, while in the background red blood cells are unaffected.

1. Introduction

Clinical diagnosis, therapeutics, and comprehensive cell biology benefit from the ability to isolate and enrich rare cells derived from a heterogeneous population (Gossett et al., 2010). Fluorescence-activated cell sorting (FACS) and magnetic-activated cell sorting (MACS) are the most commonly utilized sorting methodologies. These techniques use fluorophore-conjugated antibodies and antibody-conjugated magnetic beads to label and process target cells. Systems employing FACS and MACS provide high throughput screening; however, they have large initial and operational costs, require specialized training, may affect cell fate and function due to shear stress, the use of antibodies, and fluorophores, and requires prior knowledge about cell surface markers (Kumar and Bhardwaj, 2008). Because of this, there is a growing need for a marker-independent isolation and purification method.

A number of marker-independent methods have been developed which sort cells by exploiting unique physical phenomena which can be manipulated on the microscale including streamline manipulation (Takagi et al., 2005), microstructure flow perturbation (Choi et al., 2009), gravity (Warrick et al., 2010), and inertial forces (Di Carlo, 2009). Other methods sort cells based on their intrinsic properties including their volumetric (Vona et al., 2000), mechanical (Mohamed et al., 2009), magnetic (Huang et al., 2008), and electrical (Gascoyne et al., 2009) properties. Recently, Mach et al. demonstrated a massively parallel filtration capable device capable of isolating bacteria from blood with a flow rate of 8 mL/min using inertial forces (Mach and Di Carlo, 2010). Choi et al. were able to isolate cells based on their phase in the cell life cycle in a grooved microfluidic device (Choi et al., 2009). Mohamed et al. demonstrated the ability to isolate circulating cancer cells from whole blood based on size and deformability in a device containing pillars in stages of decreasing pillar-to-pillar spacing (Mohamed et al., 2009). These devices have obvious advantages due to their simplicity and dependence on singular physical phenomenon (i.e., hydrodynamics).

Other methods have recently been reported which improve selectivity to sort cells of similar size, but different genotype by employing electromagnetic forces. Gascoyne et al. demonstrated a tumor cell isolation efficiency of 92% in a dielectrophoresis (DEP) field flow fractionation device using an electric field generated at 60 kHz (Gascoyne et al., 2009). DEP is a phenomenon which occurs at the micro-scale when a dielectric particle is placed in a non-uniform electric field. A net force is generated due to charge distributions within the particle. This has been successfully used

* Corresponding author at: 330 ICTAS, Stanger Street, Blacksburg, VA 24061, United States. Tel.: +1 540 231 1979.
E-mail address: davalos@vt.edu (R.V. Davalos).

0956-5663/$ – see front matter © 2011 Elsevier B.V. All rights reserved.
doi:10.1016/j.bios.2011.07.048

to examine, manipulate, isolate, or enrich particles (Martinez-Lopez et al., 2009), DNA (Asbury and van den Engh, 1998; Ros et al., 2006), viruses (Muller et al., 1996), and cells (Archer et al., 1999; Hwang et al., 2009; Srivastava et al., 2008). DEP devices typically consist of metal electrodes deposited onto a glass substrate (Yang et al., 1999a). The geometry of these electrodes generates the non-uniform electric field required for DEP. Alternatively, insulator based dielectrophoresis (iDEP) devices employ insulating structures within a microfluidic channel to produce non-uniformities when electrodes are inserted into the ends of the channel (Cummings and Singh, 2003; Lapizco-Encinas et al., 2005). These devices can employ both DC and AC electric fields (Hawkins et al., 2007) and many geometric configurations including sawtooth channels (Chen et al., 2009; Staton et al., 2010).

Contactless dielectrophoresis (cDEP) devices are a new adaptation of this technique in which fluid electrodes, isolated from the main microfluidic channel by a thin membrane, provide the necessary electric field in the sample channel (Shafiee et al., 2009,2010a,b). This helps mitigate some challenges with traditional dielectrophoresis devices including fouling, bubble formation, and electrode delamination (Hughes, 2002). cDEP devices can be fabricated by replication from a single etch master stamp and can be translated to mass fabrication techniques, similar to methods used for iDEP (Sabounchi et al., 2008), while eliminating direct sample-electrode contact. The insulating barriers capacitively couple the fluid electrodes to the sample channel resulting in a complex frequency dependent electric field gradient within the sample channel. The magnitude of the electric field gradient at any frequency is dependent on the geometric and material properties of the device. This work presents a continuous sorting device which is the first cDEP design capable of exploiting the Clausius-Mossotti factor at frequencies where it is either positive or negative for different mammalian cell types. Experimental devices were fabricated using a cost effective fabrication technique which does not require the use of a cleanroom or specialized equipment. An analytical model was developed to evaluate cDEP devices as a network of parallel resistor–capacitor pairs. Two theoretical devices are presented and evaluated using finite element methods to demonstrate the effect of geometry on the development of electric field gradients across a wide frequency spectrum. Finally, we present a third experimental device capable of continuously sorting human leukemia cells from dilute blood samples.

2. Theory

The application of a voltage across conductive and dielectric materials will induce an electric field

$$\vec{E} = -\nabla\phi \tag{1}$$

where ϕ is the applied voltage. Under the influence of this electric field, dielectric particles immersed in a conductive fluid will become polarized. If the electric field is non-uniform, particles are driven towards the regions of field gradient maxima by a translational dielectrophoretic force ($\vec{F}_{\mathrm{DEP}}$) (Pohl and Plymale, 1960)

$$\vec{F}_{\mathrm{DEP}} = \gamma_{\mathrm{DEP}}\nabla\left|\vec{E}\cdot\vec{E}\right| \tag{2}$$

where γ_{DEP} is half the induced dipole moment of the particle. For a spherical particle, this quantity can be represented as:

$$\gamma_{\mathrm{DEP}} = 2\pi \in_{\mathrm{m}} r^3 Re[K(\omega)] \tag{3}$$

where r is the radius of the cell, $\in_{\mathrm{m}}$ is the relative permitivity of the suspending medium, and Re[$K(\omega)$] is the real part of the Clausius-Mossotti (C-M) factor.

$$K(\omega) = \frac{\in_{\mathrm{c}}^* - \in_{\mathrm{m}}^*}{\in_{\mathrm{c}}^* + 2\in_{\mathrm{m}}^*} \tag{4}$$

$$\in^* = \in + \frac{\sigma}{i\omega} \tag{5}$$

where $\in_{\mathrm{c}}^*$ and $\in_{\mathrm{c}}^*$ are the permittivity of the cell and suspending medium respectively, σ is the conductivity, ω is the frequency of the applied field, and $i = \sqrt{-1}$.

A particle independent DEP vector can be defined as

$$\vec{T} = \frac{\vec{F}_{\mathrm{DEP}}}{\gamma_{\mathrm{DEP}}} = \nabla\left|\vec{E}\cdot\vec{E}\right| \tag{6}$$

$$\vec{T} = \nabla\left|(-\nabla\phi)\cdot(-\nabla\phi)\right| \tag{7}$$

$$\vec{T} = \nabla\left|\left(\frac{d\phi}{dx}\right)^2 + \left(\frac{d\phi}{dy}\right)^2 + \left(\frac{d\phi}{dx}\right)^2\right| \tag{8}$$

$$\vec{T} = \begin{bmatrix} \left(\frac{d^3}{dx^3} + \frac{d^3}{dxdy^2} + \frac{d^3}{dxdz^2}\right)\hat{e}_x \\ \left(\frac{d^3}{dx^2dy} + \frac{d^3}{dy^3} + \frac{d^3}{dydz^2}\right)\hat{e}_y \\ \left(\frac{d^3}{dx^2dz} + \frac{d^3}{dy^2dz} + \frac{d^3}{dz^3}\right)\hat{e}_z \end{bmatrix}\phi^2 \tag{9}$$

where $\hat{e}_j$ is a unit vector in the j direction.

Contactless dielectrophoresis devices can be modeled analytically as five resistor-capacitor (R–C) pairs in series. R–C pairs represent the source and sink electrode channels, the two insulating barriers, and the sample channel. The current entering and leaving each of these pairs must be the same and the total impedance of each pair can be calculated using Kirchhoff's current law and Ohm's Law.

$$Z = \frac{X_{\mathrm{c}}^2 R - iX_{\mathrm{c}}R^2}{R^2 + X_{\mathrm{c}}^2} \tag{10}$$

$$X_{\mathrm{c}} = \frac{-1}{\omega C} \tag{11}$$

Z is the total impedance of the resistor–capacitor pair, X_{c} is the capacitive reactance, C is the capacitance, and R is the resistance.

The physical geometry and the material properties of the materials present in this system influence the resistance ($R = \rho L/A$) and capacitance ($C = \in_0 \in_r A/d$) of each element where ρ and $\in_{\mathrm{r}}$ are the resistivity and relative static permittivity of the material respectively, A is the cross-sectional area, L is the length of the resistor and d is the separation distance between two conductive components. It should be noted that for the insulating membranes in a traditional cDEP device, $L = d$.

3. Methods

3.1. Clausius-Mossotti factor analytical model

The Clausius-Mossotti factor for THP-1 human leukemia monocytes and red blood cells (RBC) was modeled over a logarithmic distribution between 100 Hz and 100 MHz using MATLAB (Version R2010a, MathWorks Inc., Natick, MA, USA). Dispersing cytoplasmic properties which effect high frequency behavior were modeled for RBCs as presented by Gimsa et al. (1996). In this method, the conductivity and permittivity of the cell were influenced by an additional dispersion term σ_{c} and $\in_{\mathrm{c}}$ respectively.

$$\sigma_{\mathrm{c}} = \sigma_{\mathrm{co}} + \Delta\sigma\frac{(\omega\tau_{\mathrm{c}})^{2(1-\alpha)}}{(1+\omega\tau_{\mathrm{c}})^{2(1-\alpha)}} \tag{12}$$

$$\in_{\mathrm{c}} = \in_{\mathrm{c}\infty} + \Delta\in_{\mathrm{r}}\left(\frac{1}{(1+\omega\tau_{\mathrm{c}})^{2(1-\alpha)}}\right) \tag{13}$$

$\in_{\mathrm{c}\infty}$ and σ_{co} are the high frequency permittivity and initial conductivity of the cytoplasm, $\Delta\in_{\mathrm{r}}$ and σ_{r} are frequency dependant

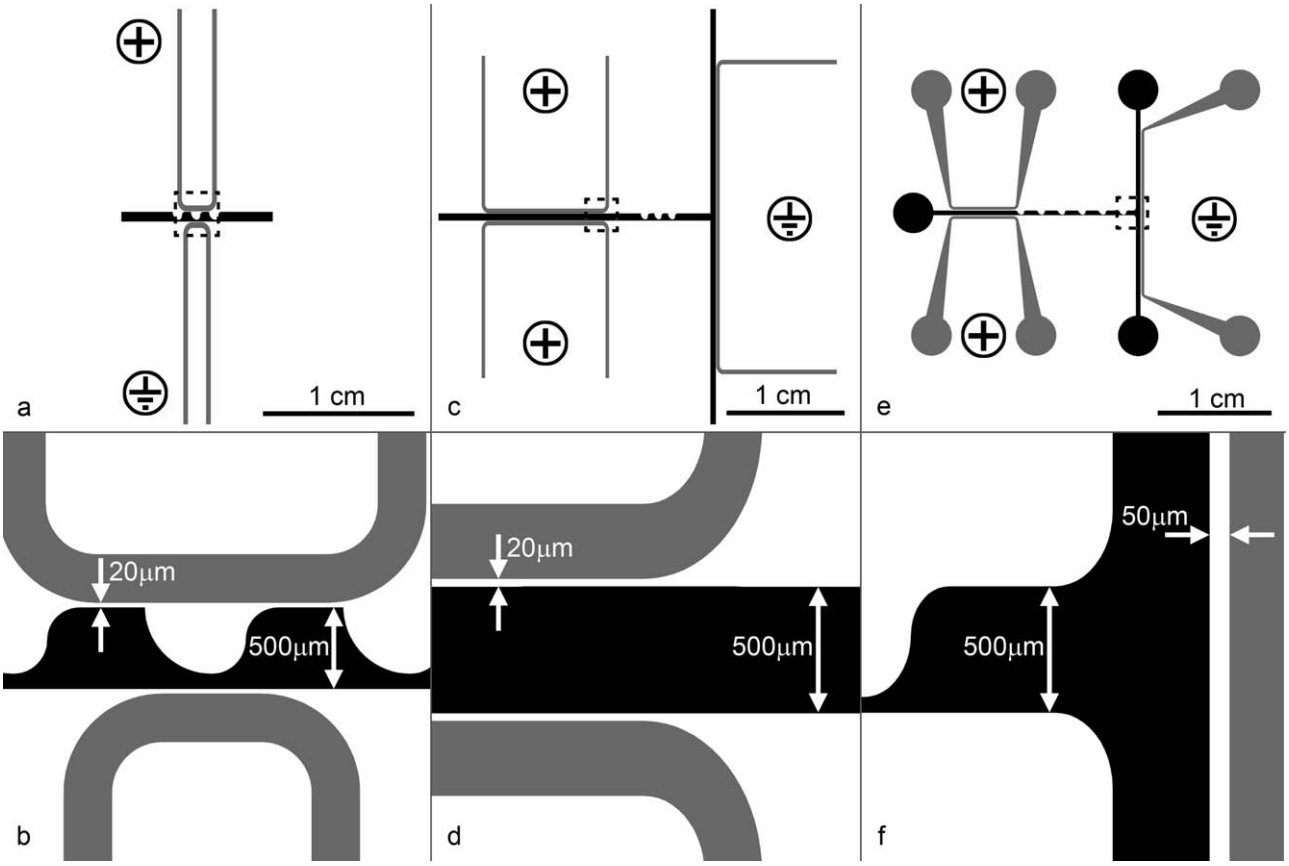

Fig. 1. Schematics for (a and b) Device 1, (c and d) Device 2, and (e and f) Device 3. Device 1 has geometrical feature sizes similar to traditional cDEP devices reported in the literature. The total barrier length and distance between source and sink electrodes is increased in Devices 2 and 3. Fluid electrode channels (gray) had boundary conditions of 100 V and ground applied at their inlets as shown above.

ratios of change, α is the distribution range of dispersion frequencies, and τ_c is the cytoplasmic time constant.

$$\tau_c = \frac{\in_c}{\sigma_c} \tag{14}$$

The values used in these models can be found in Table 1.

3.2. Device design

Three cDEP devices were devised to numerically evaluate the $\vec{T}$ frequency response and the impedance of the fluid electrodes, sample channel, and insulating barriers between 10 Hz and 100 MHz. The third device was further used to validate the numerical model experimentally. Design 1, Fig. 1a and b, has geometric features similar to previously reported devices (Shafiee et al., 2010b). These previous designs typically have a limited bandwidth in which cells can be manipulated and Device 1 served as a baseline for comparison with traditional cDEP devices. Specifically, the device is designed with fluid electrodes that are separated from each side of the sample channel by 20 μm. The fluid electrodes are 4.2 cm long, 300 μm wide, and 50 μm deep. The sample channel has maximum and minimum widths of 500 and 100 μm, respectively, which makes the channel appear to have rounded 'saw tooth' features that protrude into the channel. The insulating barriers, which separate the fluid electrodes from the sample channel, are 20 μm wide and travel along the top and bottom of the sample channel for 600 μm for a total barrier length of 0.12 cm.

Design 2, Fig. 1c–d, incorporates physical features to expand the $\vec{T}$ frequency response. The fluid electrodes are 10 cm long, 300 μm wide, and 50 μm deep. The sample channel retains the same geometric 'saw tooth' features as Design 1, however, the source and sink electrode channels are positioned such that there is a 1 cm distance between them. The sample channel then forms a 'T' junction along the right side. The insulating barriers which separate the fluid electrodes from the sample channel are 20 μm wide. The total length in which the barriers are 20 μm wide is 1 cm on the left top and bottom (source) and 2 cm along the right side (sink) for a total barrier length of 4 cm.

Design 3, Fig. 1d–e, was created for experimental validation of the numerical and analytical results presented below. This design contains the same 'saw-tooth' features as the previous designs, with three additional teeth to increase the total duration in which cell are exposed to electric field gradients. The overall device geometry is similar to Device 2, but has been modified to conform to the minimum feature size of 40 μm possible with the fabrication process presented in Sections 3.4 and A.1. The sample channel has a nominal width of 500 μm with constrictions from the 'saw-teeth' reducing the width to 100 μm. The sample channel forms a 'T' junction along the right side with approximately 1.2 cm between the source and sink electrodes. There are two source electrode channels which are each approximately 3 cm long with a minimum width of 300 μm. The barriers separating the source electrodes from the sample channel are 50 μm thick for approximately 5.8 mm on top and bottom. The sink electrode channel is approximately 3.7 cm long with a minimum width of 300 μm. The barrier separating the sink electrode channel from the sample channel is 50 μm thick for approximately 1.6 cm. The total barrier length for Design 3 is approximately 2.78 cm.

3.3. Analytical and numerical device modeling

The geometric features of Devices 1 and 2 were used to create lumped element representations for the electrode channels, insulating barriers, and the sample channel by calculating their associated resistances and capacitances. Three dimensional geometries were created using Autocad (AutocadMechanical 2010, Autodesk Inc, San Rafael, CA, USA). The geometries were imported into COMSOL Multiphysics (Version 4.0, Comsol Inc., Burlington, MA, USA) and the AC/DC module was used to solve for the potential distribution, ϕ, using the governing equation $\nabla \cdot (\sigma^* \nabla \phi) = 0$ where σ^* is the complex conductivity ($\sigma^* = \sigma + i\omega\in$). Edges of the electrode channels were modeled as a uniform potential of 100 V and ground as depicted in Fig. 1. The frequency of the applied signal was incrementally increased from 100 Hz to 10^9 Hz using the MATLAB to create a logarithmically distributed frequency distribution. Physical regions within the model were set to represent poly(dimethylsiloxane) (PDMS) (Sylgard 184, Dow Corning, USA), phosphate buffer solution (PBS), or sample media. ϕ was used to calculate the magnitude of the particle independent DEP force vector $\left(\left|\vec{T}\right|\right)$.

PDMS was defined as having a conductivity (σ) of 0.83×10^{-12} S/m and a relative permittivity (ε_r) of 2.65 as provided by the manufacturer. PBS was modeled as having a conductivity of 1.4 S/m and a relative permittivity of 80 as measured and assumed based on water composition, respectively. The conductivity of the sample was 100 μS/cm and the permittivity was also assumed to be 80.

3.4. Device fabrication

Briefly, a thin film photoresist (#146DFR-4, MG Chemicals, Surrey, British Colombia, Canada) was laminated onto glass microscope slides. The laminated slides were exposed to ultraviolet (UV) light through a film transparency mask (Output City, Cad/Art Services Inc., Bandon, OR) using an array of UV light emitting diodes and a custom exposure frame. The slides were then developed in negative photo developer (#4170-500ML, MG Chemicals, Surrey, British Columbia, Canada) and used as a master stamp for PDMS replication. The PDMS molds were bonded to the glass slides after treating with air plasma (Harrick Plasma, Ithaca, New York). For a full description of this process, see supplementary data in section A.1.

3.5. Cell preparation

The live samples of THP-1 human leukemia monocytes (American Type Culture Collection, Manassas, VA, USA) were washed twice and resuspended in a buffer used for experiments (8.5% sucrose [wt/vol], 0.3% glucose [wt/vol], and 0.725% [wt/vol] RPMI (Flanagan et al., 2008)) to 1×10^6 cells/mL. THP-1 cells were stained using a LIVE/DEAD® Viability/Cytotoxicity Kit for mammalian cells (Molecular Probes Inc., Carlsbad, CA, USA). Calcein Red/Orange, which is enzymatically converted to fluorescent calcein, was added to the sample at 2 μL per mL of cell suspension. A drop of whole blood, obtained via a diabetic finger stick from willing volunteers, was added to 5 mL of buffer. The suspension was then diluted to achieve a red blood cell concentration of 1×10^7 cells.

The two cell samples were then vortexed for 5 min, washed once and resuspended in buffer. The THP-1 and RBC suspensions were then mixed together in one conical tube with a final concentration of 1×10^6 and 1×10^7 cells/mL, respectively. The buffer had a final conductivity of 100–115 μS/cm measured with a SevenGo Pro conductivity meter (Mettler-Toledo, Inc., Columbus, OH, USA).

3.6. Experimental setup

A syringe pump was used to drive samples at a rate of 0.01 mL/h (PHD Ultra, Harvard Apparatus, Holliston, MA, USA). An AC electric field was created by amplifying (AL-50HF-A, Amp-Line Corp., Oakland Gardens, NY, USA) the output signal of a function generator (GFG-3015, GW Instek, Taipei, Taiwan). A step up transformer was used to achieve output voltages up to 300 V_{RMS} between 50 and 100 kHz. Voltage and frequency were measured using an oscilloscope (TDS-1002B, Tektronics Inc. Beaverton, OR, USA) connected to the output stage of the transformer.

4. Results and discussion

4.1. Analytical method

Cells are repelled from regions of maximal electric field gradient at frequencies where C-M factor is negative. Conversely, when the C-M factor is positive, cells are driven towards regions of maximal electric field gradient. Mammalian cells exhibit a negative C-M factor at low frequencies. As frequency increases, the C-M factor begins to increase, crossing into the positive domain at frequencies on the order of 1 kHz. The lowest frequency at which the C-M factor is exactly zero is known as the first crossover frequency. The magnitude of the C-M factor changes drastically in proximity to the first crossover frequency and it is expected that in this region, cells of similar genotypes will be most easily discriminated.

Over a majority of the frequency spectrum, the C-M factor for THP-1 cells and RBCs is of similar magnitude and direction as seen in Fig. 2a. In these regions, the resulting DEP force will tend to drive both cell types into similar regions. This action is intrinsic and is independent of device geometry. At frequencies between 20 kHz

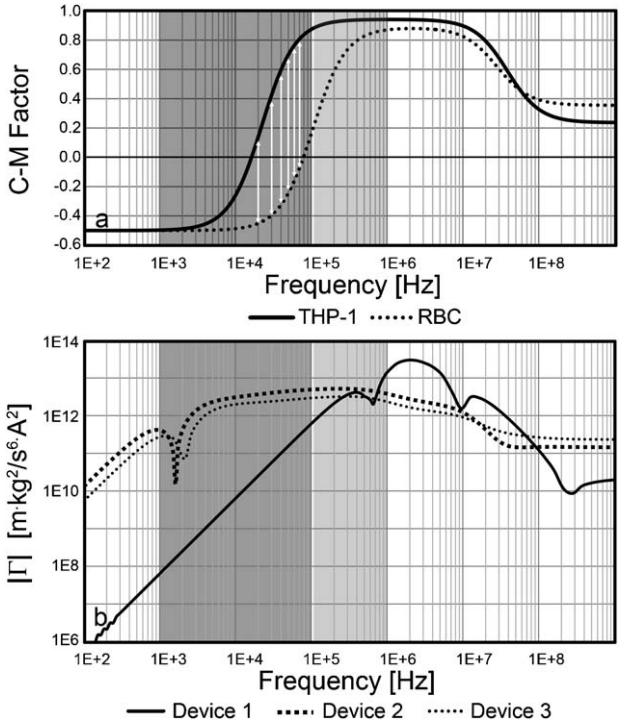

Fig. 2. cDEP devices can be optimized to develop high $\left|\vec{T}\right|$ values at low frequencies. (a) THP-1 and RBCs have unique Clausius-Mossotti factor curves. The white arrows show regions where the C-M factor for THP-1 cells is positive while the C-M factor for RBCs is negative. (b) Device 2 and 3 generate significantly higher electric field gradients near the first C-M factor crossover frequency. The light and dark gray regions show the operating frequencies for traditional cDEP devices and the optimal cDEP operating frequencies, respectively.

and 70 kHz the C-M factors for THP-1 and RBCs are opposite, as indicated by the white arrows. This indicates that a DEP force will move the cells in opposite directions. Between 70 kHz and 500 kHz the C-M factor is of similar direction, but of greater magnitude for THP-1 cells. It is important to note that if the conductivity of the buffer solution is increased, these regions will shift and occur at higher frequencies. The light gray region of Fig. 2a depicts the typical frequencies over which cDEP devices are able to manipulate cells. The dark gray region represents the ideal operating range over which mammalian cells of different genotypes will likely have distinct C-M factors.

The particle independent DEP force vector $\left(\left|\vec{T}\right|\right)$ is highly dependent on the voltage drop within the sample channel. The dielectric breakdown of PDMS limits the magnitude of experimental voltages; therefore, it is important that a large proportion of the total voltage drop across the device occurs across the sample channel. In a traditional cDEP device, represented by Device 1, the impedance of the insulating barriers dominates the sample and electrode channels. This results in a large voltage drop across the insulating barriers at low frequencies. As shown in Fig. 3a, the capacitive nature of the barrier causes its impedance to decrease with increasing frequency. These devices are able to manipulate cells and particles at frequencies above 100 kHz (Shafiee et al., 2010b), when approximately 1% of the total voltage drop occurs across the sample channel.

Device 2 represents a cDEP device with geometric features that increase barrier capacitance and sample channel resistance. This causes the impedance of the barriers to roll off at lower frequencies and increase the proportion of voltage drop across the sample channel as shown in Fig. 3b. In this geometry, 1% of the total voltage drop occurs across the sample channel at approximately 100 Hz. At frequencies of 1, 10, 100, and 1000 kHz, the voltage drop across the sample channel is 0.01, 0.12, 1.16, and 9.40 percent, respectively, of the total voltage drop across Device 1. In contrast, at the same frequencies, the voltage drop across the sample channel of Device 2 is 8.54, 45.97, 81.67, and 88.50 percent respectively. This shows that the geometric properties of cDEP devices can be manipulated to reduce the impedance of the insulating barriers and increase the total voltage drop across the sample channel. This is important due to the high dependence of Γ on the magnitude and spatial changes of the voltage.

The electrode and sample channels have relatively small capacitive components, which are omitted in Fig. 3c. This additional capacitance causes the impedance of these elements to roll off at frequencies above 10 MHz as shown in Fig. 3a and b. At frequencies above 10 MHz, the materials begin to appear homogeneous, and the ability of cDEP devices to produce useful electric field gradients may be diminished.

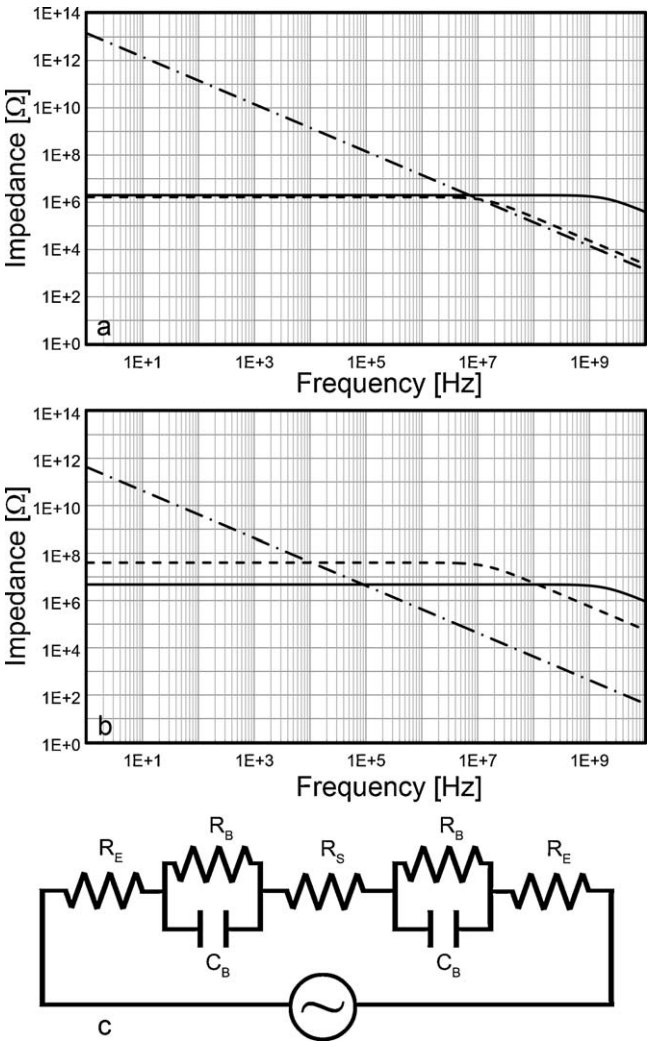

Fig. 3. The frequency response of cDEP devices can be improved by altering the geometry. (a) The impedance of the insulating barriers in a traditional cDEP device (Device 1) results in small voltage drops across the sample channel. (b) The geometry can be altered (Device 2) to increase the sample channel voltage drop at frequencies near the first C-M Factor cross over point. The solid, dashed, and dash-dotted lines represent the impedance of the electrode channels, sample channel, and insulating barriers, respectively. (c) Simplified cDEP resistor-capacitor analytical network.

4.2. Numerical method

Previously reported cDEP devices demonstrated the ability to manipulate cells and particles with numerically calculated Γ values of 1×10^{-12} or greater (Shafiee et al., 2009,2010a,b). This value is used here as a minimum threshold representing the ability of a theoretical cDEP device to manipulate cells. As shown in Fig. 2b, the electric field gradient of Device 1 reaches this magnitude, at approximately 100 kHz. This is consistent with results reported previously (Shafiee et al., 2010b) for traditional cDEP devices. Between 1 and 10 MHz, the electric field gradient developed within the sample channel increases to above $1 \times 10^{-13}[\mathrm{m\,kg^2\,s^{-6}\,A^{-2}}]$, however, in this range, the C-M factor is expected to drop towards zero reducing the total DEP force. Additionally, the generation of high voltage signals at these frequencies is difficult and requires specialized equipment. The light gray region of Fig. 2b depicts the typical frequency range over which traditional cDEP devices achieve particle isolation and enrichment (Shafiee et al., 2009,2010a,b).

The electric field gradient within the sample channel of Device 2 is above $1 \times 10^{-12}[\mathrm{m\,kg^2\,s^{-6}\,A^{-2}}]$ between 3 kHz and 10 MHz. Within this frequency range, the electric field gradient is similar to that reported for traditional cDEP devices capable of isolating live from dead cells (Shafiee et al., 2010b). The electric field gradient produced in Device 2 is of significant magnitude to manipulate cells while the C-M factor is close to the first crossover frequency for THP-1 cells. These results effectively demonstrate that the geometric features of a cDEP device can be modified so that cells can be manipulated using both positive and negative DEP.

At 50 kHz, the lower limit of our electronics' capabilities, Device 1 does not generate an electric field gradient above $1 \times 10^{-12}[\mathrm{m\,kg^2\,s^{-6}\,A^{-2}}]$, as shown in Fig. 4a. In contrast, Device 2 generates electric field gradients in excess of $5 \times 10^{-12}[\mathrm{m\,kg^2\,s^{-6}\,A^{-2}}]$ in regions close to the 'saw-tooth' features. Fig. 4b shows the regions of high electric field gradient within Device 2. The asymmetrical features create regions of highest electric field gradient proximal to the top of the sample channel.

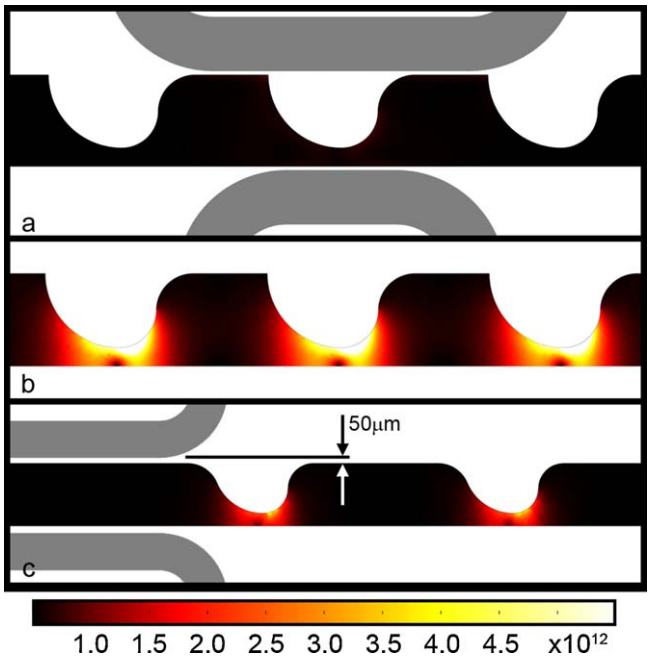

Fig. 4. Geometric features impact device performance. At 100 V_{RMS} (a) Device 1 fails to generate a significant electric field gradient at 50 kHz as a result of small barrier capacitance and sample channel resistance. (b) Device 2 produces higher electric field gradients due to its longer barriers and increased distance between source and sink electrodes. (c) Device 3 produces significant electric field gradients at 50 kHz. The legend depicts the value of $\left|\vec{T}\right|$ in units of [m kg^2 s^{-6} A^{-2}]. (For interpretation of the references to color in this figure legend, the reader is referred to the web version of the article.)

Numerical analysis of Device 3, Fig. 4c, shows that the device is capable of generating an electric field gradient above 1×10^{-12}[m kg^2 s^{-6} A^{-2}] at 50 kHz. Fig. 4c shows that Device 3 produces an asymmetrical electric field gradient of similar shape but lower magnitude compared to Device 2. The electric field gradient within the sample channel of Device 3 is above 1×10^{-12}[m kg^2 s^{-6} A^{-2}] between 4 kHz and 10 MHz as shown in Fig. 2b.

4.3. Experimental validation

Microfluidic channels 50 μm and greater in width can be repeatedly produced using the process described. This directly matches the photoresist manufacturer's specifications. Narrower features failed to develop smooth and well defined lines (results not shown). Channels separated by 40 μm or greater could be fully developed and PDMS replication resulted in water tight bonds between parallel channels. Higher resolution photoresist films could be used to reduce the minimum feature sizes; however, many of these films are only available in industrial quantities and were not evaluated.

In the absence of an applied electric field, THP-1 cells and RBCs passed freely through Device 3 without being affected as shown in Fig. 5a. When 231 V_{RMS} at 50 kHz was applied, 'pearl chain' formation of THP cells, indicative of DEP, was initially observed. Cells then began to slowly migrate from the bottom of the sample channel towards the top wall. THP-1 cells which were in the sample channel prior to the application of the electric field continued to exit the device through the top and bottom paths of the 'T-channel'. After approximately 1 min, all of the initial cells had passed through the device and new cells were reaching the 'T-intersection'. These cells had experienced a DEP force the entire distance between the electrodes and most were exiting only through the top path of the 'T-channel'. At this voltage and frequency, shown in Fig. 5b, THP-1

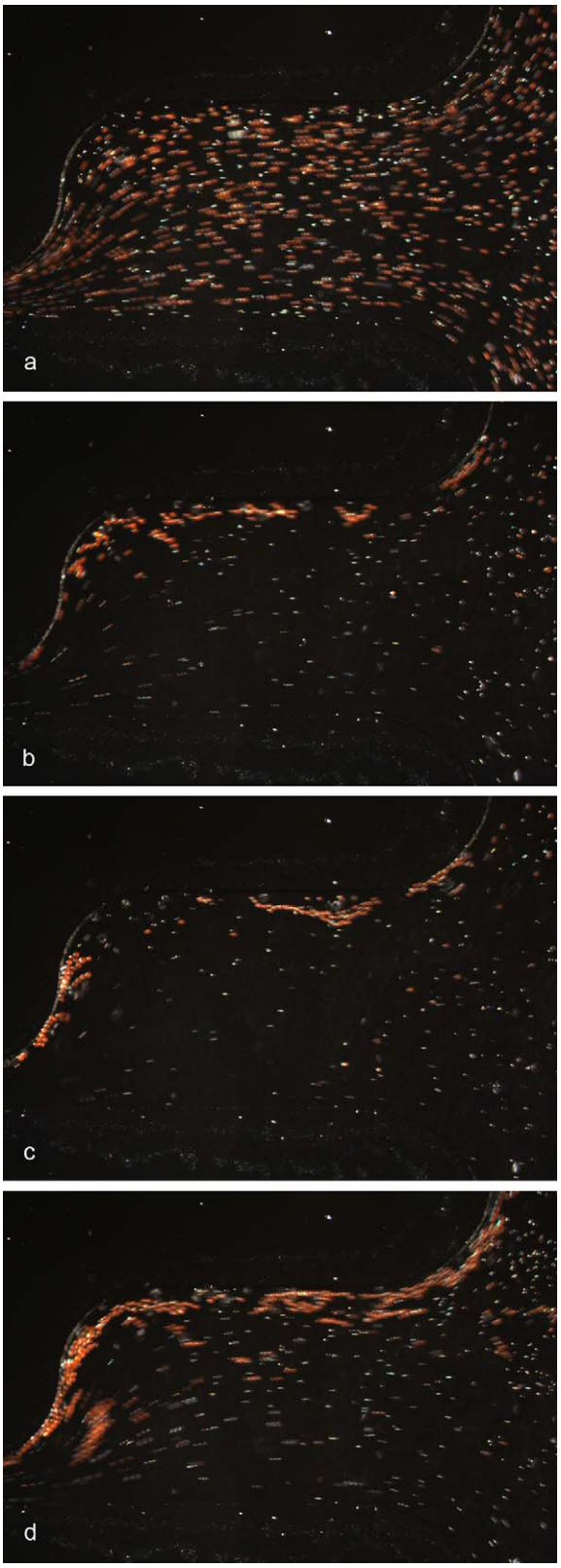

Fig. 5. THP-1 cell can be sorted from a heterogeneous population. Cell pass through the device with a uniform distribution when (a) the electric field is turned off. (b) However, THP-1 cells are attracted towards regions at the top of the sample channel while RBCs pass through unaffected when 231 V_{RMS} at 50 kHz, (c) 227 V_{RMS} at 70 kHz, and (d) 234 V_{RMS} 90 kHz is applied.

Table 1
Dielectric properties used to calculate the C-M factor for THP-1 and RBCs. Values derived from ‡(Gimsa et al., 1996), †(Pethig and Kell, 1987), *(Holmes et al., 2003), +(Yang et al., 1999b), ^assumption based on water content, and #measured values.

	THP-1	RBC	
$\in_m$	$80\varepsilon_0$^	$80\varepsilon_0$^	
$\in_c$	154.4+	212‡	
σ_m	0.01#	0.01#	(S/m)
σ_c	0.65+	0.4‡	(S/m)
c_m	0.0177*	0.00997‡	(F/m^2)
$\Delta\in_r$	–	162‡	
$\Delta\sigma_r$	–	0.135‡	(S/m)
α	–	0†	
$\in_{c\infty}$	–	$50\varepsilon_0$‡	

cells did not become trapped near the saw-tooth features and continued to travel along the upper channel wall while RBCs passed through the device unaffected. Similar results were observed at 60 kHz.

Between 70 and 100 kHz, THP-1 cells formed pearl chains and migrated towards the top wall of the sample channel when 250 V_{RMS} or greater was applied. Additionally, some chains began to trap near the saw-tooth features as shown in Fig. 5c and d. At 80 to 100 kHz a small number of cells began to decrease in fluorescence, indicative of electroporation or cell damage (Bao et al., 2010). The number of cells trapping increased with both increasing applied voltage and frequency. Enrichment and entrapment of THP-1 at 80 kHz and 234 V_{RMS} can be seen in Video 1.

The purpose of the devices presented above was to demonstrate the theoretical ability of cDEP to function at low frequencies. The experimental results presented validate the approach and establish that the contactless dielectrophoresis platform is capable of manipulating cells at frequencies below 100 kHz in physiologically suitable buffers. Operating at these low frequencies will allow for the manipulation of cells using negative dielectrophoresis, a task previously unachievable using cDEP. At frequencies between 50 and 90 kHz a large positive DEP force was observed acting on the human leukemia cells. At 50 kHz, theory predicts that the Clausius-Mossotti factor for RBCs is slightly negative. This in conjunction with their smaller size resulted in the observation of a negligible negative DEP force. It is expected that at lower frequencies a more dominant negative DEP force will act on the RBCs while a positive force continues to act on the THP-1 cells. The combination of these opposing forces may split the cells into separate streams for collection.

Alternatively, the geometry of the outlet channels could be modified such that the bifurcation at the end of the sample channel splits the flow into two non-equal branches as shown in Fig A.3. A small portion of the flow containing the cancer cells would be allowed to flow towards the upper outlet, and the remaining flow containing the majority of the RBCs would be directed towards the lower outlet. This change in geometry could alleviate the need for a strong negative DEP force acting on the RBCs as they would only need to be forced from the top portion of the channel. In this geometry, the Zweifach-Fung effect, in which particle fraction tends to increase in the high-flow-rate branch (Doyeux et al., 2011), could increase sorting purity since a small negative DEP force acting on the RBCs would cause a depletion region near the walls.

5. Conclusion

The fabrication technique presented here has been used to successfully demonstrate the first cDEP device with insulating barriers greater than 20 μm. The low cost of fabrication, simplicity, availability of supplies, and exclusion of toxic chemicals make this technique ideal for researchers that do not have access to a cleanroom. Furthermore, this process displays potential as a rapid, low cost solution for the fabrication of complex multi-phased devices capable of sorting, isolating, and enriching samples as well as performing downstream analysis, such as impedance detection. In contrast to traditional cell sorting technologies such as FACS and MACS, the single stamp fabrication and associated electronics do not require specialized equipment and have a relatively low cost of entrance. Additionally, cDEP does not require the use of surface markers, dyes, or antibodies which require substantial prior knowledge of the cell's biology.

Traditional cDEP devices are capable of developing the electric field gradients necessary for dielectrophoretic manipulation between 100 kHz and 1 MHz. The frequency dependent behavior of cDEP devices creates a unique set of challenges in manipulating mammalian cells. The first crossover frequency for many cells is anticipated to be below this frequency range for low conductivity sample buffers. Additionally, cells of similar genotypes may have crossover frequencies which occur within a narrow frequency range. Since the C-M factor for these cells may not differ significantly except in proximity to the crossover frequencies, it is paramount that future cDEP devices be capable of manipulating particles between 1 and 100 kHz.

Numerical results indicate that these devices will continue to develop useful DEP forces at frequencies as low as 1 kHz. This is advantageous because systems designed to operate above 100 kHz and 100 V_{RMS} require custom electronics and magnetics. Preliminary experiments with RBCs, macrophages, leukemia monocytes, prostate and breast cancer cells (results not shown) indicate that between 50 and 100 kHz RBCs and macrophages experience a negligible DEP response. Meanwhile, the leukemia, breast, and prostate cancer cells exhibit a strong positive DEP response which forces them into the top half of the channel. The ability of this device to separate low concentrations cancer cells from other common subpopulations found in blood will be the emphasis of future studies. Future work will focus on the development of complementary electronics, demonstration of a positive DEP response for THP-1 cells, a concurrent negative DEP response for RBCs resulting in continuous isolation of the two populations and quantification of selectivity, enrichment factor, and cell viability.

Conflicts of Interest

The authors have a pending patent for contactless dielectrophoresis.

Acknowledgements

This work was supported in part by the Institute for Critical Technology and Applied Science (ICTAS) at Virginia Tech. The authors would like to thank the members of the BEMS laboratory, especially Andrea Rojas and Roberto C. Gallo-Villanueva, for their help with editing this document.

Appendix A. Supplementary data

Supplementary data associated with this article can be found, in the online version, at doi:10.1016/j.bios.2011.07.048.

References

Archer, S., Li, T.T., Evans, A.T., Britland, S.T., Morgan, H., 1999. Biochem. Biophys. Res. Commun. 257 (3), 687–698.
Asbury, C.L., van den Engh, G., 1998. Biophys. J. 74 (2), 1024–1030.
Bao, N., Le, T.T., Cheng, J.-X., Lu, C., 2010. Integr. Biol. 2 (2-3), 113–120.
Chen, K.P., Pacheco, J.R., Hayes, M.A., Staton, S.J.R., 2009. Electrophoresis 30 (9), 1441–1448.

Choi, S., Song, S., Choi, C., Park, J.K., 2009. Anal. Chem. 81 (5), 1964–1968.
Cummings, E.B., Singh, A.K., 2003. Anal. Chem. 75 (18), 4724–4731.
Di Carlo, D., 2009. Lab on a Chip 9 (21), 3038–3046.
Doyeux, V., Podgorski, T., Peponas, S., Ismail, M., Coupier, G., 2011. J. Fluid Mech. 674, 359–388.
Flanagan, L.A., Lu, J., Wang, L., Marchenko, S.A., Jeon, N.L., Lee, A.P., Monuki, E.S., 2008. Stem Cells 26 (3), 656–665.
Gascoyne, P.R.C., Noshari, J., Anderson, T.J., Becker, F.F., 2009. Electrophoresis 30 (8), 1388–1398.
Gimsa, J., Muller, T., Schnelle, T., Fuhr, G., 1996. Biophys. J. 71 (1), 495–506.
Gossett, D.R., Weaver, W.M., Mach, A.J., Hur, S.C., Tse, H.T.K., Lee, W., Amini, H., Di Carlo, D., 2010. Anal. Bioanal. Chem. 397 (8), 3249–3267.
Hawkins, B.G., Smith, A.E., Syed, Y.A., Kirby, B.J., 2007. Anal. Chem. 79 (19), 7291–7300.
Holmes, D., Green, N.G., Morgan, H., 2003. IEEE Eng. Med. Biol. Mag. 22 (6), 85–90.
Huang, R., Barber, T.A., Schmidt, M.A., Tompkins, R.G., Toner, M., Bianchi, D.W., Kapur, R., Flejter, W.L., 2008. Prenat. Diagn. 28 (10), 892–899.
Hughes, M.P., 2002. Electrophoresis 23 (16), 2569–2582.
Hwang, H., Lee, D.H., Choi, W.J., Park, J.K., 2009. Biomicrofluidics 3 (1).
Kumar, A., Bhardwaj, A., 2008. Biomed. Mater. 3 (3).
Lapizco-Encinas, B.H., Davalos, R.V., Simmons, B.A., Cummings, E.B., Fintschenko, Y., 2005. J. Microbiol. Methods 62 (3), 317–326.
Mach, A.J., Di Carlo, D., 2010. Biotechnol. Bioeng. 107 (2), 302–311.
Martinez-Lopez, J.I., Moncada-Hernandez, H., Baylon-Cardiel, J.L., Martinez-Chapa, S.O., Rito-Palomares, M., Lapizco-Encinas, B.H., 2009. Anal. Bioanal. Chem. 394 (1), 293–302.
Mohamed, H., Murray, M., Turner, J.N., Caggana, M., 2009. J. Chromatogr. A 1216 (47), 8289–8295.
Muller, T., Fiedler, S., Schnelle, T., Ludwig, K., Jung, H., Fuhr, G., 1996. Biotechnol Technol. 10 (4), 221–226.
Pethig, R., Kell, D.B., 1987. Phys. Med. Biol. 32 (8), 933–970.
Pohl, H.A., Plymale, C.E., 1960. J. Electrochem. Soc. 107 (5), 390–396.
Ros, A., Hellmich, W., Regtmeier, J., Duong, T.T., Anselmetti, D., 2006. Electrophoresis 27 (13), 2651–2658.
Sabounchi, P., Morales, A.M., Ponce, P., Lee, L.P., Simmons, B.A., Davalos, R.V., 2008. Biomed. Microdevices 10 (5), 661–670.
Shafiee, H., Caldwell, J.L., Davalos, R.V., 2010a. Jala 15 (3), 224–232.
Shafiee, H., Caldwell, J.L., Sano, M.B., Davalos, R.V., 2009. Biomed. Microdevices 11 (5), 997–1006.
Shafiee, H., Sano, M.B., Henslee, E.A., Caldwell, J.L., Davalos, R.V., 2010b. Lab on a Chip.
Srivastava, S.K., Daggolu, P.R., Burgess, S.C., Minerick, A.R., 2008. Electrophoresis 29 (24), 5033–5046.
Staton, S.J.R., Chen, K.P., Taylor, T.J., Pacheco, J.R., Hayes, M.A., 2010. Electrophoresis 31 (22), 3634–3641.
Takagi, J., Yamada, M., Yasuda, M., Seki, M., 2005. Lab on a Chip 5 (7), 778–784.
Vona, G., Sabile, A., Louha, M., Sitruk, V., Romana, S., Schutze, K., Capron, F., Franco, D., Pazzagli, M., Vekemans, M., Lacour, B., Brechot, C., Paterlini-Brechot, P., 2000. Am. J. Pathol. 156 (1), 57–63.
Warrick, J., Casavant, B., Frisk, M., Beebe, D., 2010. Anal. Chem. 82 (19), 8320–8326.
Yang, J., Huang, Y., Wang, X.B., Becker, F.F., Gascoyne, P.R.C., 1999a. Anal. Chem. 71 (5), 911–918.
Yang, J., Huang, Y., Wang, X.J., Wang, X.B., Becker, F.F., Gascoyne, P.R.C., 1999b. Biophys. J. 76 (6), 3307–3314.